nature medicine

LETTERS

Direct evidence for cancer-cell-autonomous extracellular protein catabolism in pancreatic tumors

Shawn M Davidson[1–3,13], Oliver Jonas[1,4,13], Mark A Keibler[5], Han Wei Hou[6], Alba Luengo[1,2], Jared R Mayers[1,2], Jeffrey Wyckoff[1], Amanda M Del Rosario[1], Matthew Whitman[1], Christopher R Chin[1], Kendall J Condon[2], Alex Lammers[1], Katherine A Kellersberger[7], Brian K Stall[7], Gregory Stephanopoulos[5], Dafna Bar-Sagi[8], Jongyoon Han[6,9], Joshua D Rabinowitz[10], Michael J Cima[1,11], Robert Langer[1,5] & Matthew G Vander Heiden[1–3,12]

Mammalian tissues rely on a variety of nutrients to support their physiological functions[1]. It is known that altered metabolism is involved in the pathogenesis of cancer, but which nutrients support the inappropriate growth of intact malignant tumors is incompletely understood[2,3]. Amino acids are essential nutrients for many cancer cells[4,5] that can be obtained through the scavenging and catabolism of extracellular protein via macropinocytosis[6,7]. In particular, macropinocytosis can be a nutrient source for pancreatic cancer cells, but it is not fully understood how the tumor environment influences metabolic phenotypes[8] and whether macropinocytosis supports the maintenance of amino acid levels within pancreatic tumors. Here we utilize miniaturized plasma exchange to deliver labeled albumin to tissues in live mice, and we demonstrate that breakdown of albumin contributes to the supply of free amino acids in pancreatic tumors. We also deliver albumin directly into tumors using an implantable microdevice, which was adapted and modified from ref. 9. Following implantation, we directly observe protein catabolism and macropinocytosis *in situ* by pancreatic cancer cells, but not by adjacent, non-cancerous pancreatic tissue. In addition, we find that intratumoral inhibition of macropinocytosis decreases amino acid levels. Taken together, these data suggest that pancreatic cancer cells consume extracellular protein, including albumin, and that this consumption serves as an important source of amino acids for pancreatic cancer cells *in vivo*.

Albumin is the most abundant extracellular protein in blood and in tissues, and has been previously shown to be internalized into the lysosomes of cells in tumors[10,11]. Hypoalbuminemia is observed in many patients with cancer, and epidemiological studies suggest that the levels of serum albumin present in a patient before treatment are associated with differences in survival[12,13]. Decreased albumin levels observed in the blood of human patients with cancer and tumor-bearing animals have been posited to result from decreased hepatic synthesis or increased degradation, either by the liver or other organs such as skeletal muscle[14–17]. Direct catabolism of albumin by the tumor itself might also contribute to hypoalbuminemia, but the extent to which this catabolism occurs *in vivo* remains controversial owing to the lack of reliable methods that are able to trace albumin fate.

Macropinocytosis is a conserved, actin-dependent and endocytic process that results in nonspecific bulk internalization of extracellular material, including protein and other macromolecules, into the cell[6,7,18]. Pharmacological and genetic inhibition of macropinocytosis can inhibit cell line proliferation and xenograft tumor growth, presenting a potential therapeutic target for a subset of tumors, including some driven by oncogenic *KRAS*[6,7]. Protein scavenging has been put forth as a mechanism of nutrient acquisition on the basis of the elevated levels of amino acids observed in human pancreatic tumors[6], but direct evidence that protein is catabolized *in vivo* in a tumor-autonomous manner is lacking.

We produced mouse serum albumin where amino acids were labeled with a stable nitrogen isotope ([^{15}N]MSA) using the yeast *Pichia pastoris*[18–20] (**Supplementary Fig. 1a–c**) to determine whether albumin could be used as a nutrient source for tumors *in vivo*. Exchanging endogenous albumin in the plasma for labeled albumin is necessary for the purposes of this study to achieve sufficient enrichment of labeled protein over reasonable infusion times to allow the fate of labeled albumin in tissues to be traced. Because albumin has a large volume of distribution in the body and has slow turnover (approximately 1–2% of total albumin per day)[12,21], we designed a plasmapheresis approach to exchange endogenous albumin for [^{15}N]MSA using a

[1]Koch Institute for Integrative Cancer Research, Massachusetts Institute of Technology, Cambridge, Massachusetts, USA. [2]Department of Biology, Massachusetts Institute of Technology, Cambridge, Massachusetts, USA. [3]Broad Institute of MIT and Harvard University, Cambridge, Massachusetts, USA. [4]Department of Radiology, Brigham and Women's Hospital and Harvard Medical School, Cambridge, Massachusetts, USA. [5]Department of Chemical Engineering, Massachusetts Institute of Technology, Cambridge, Massachusetts, USA. [6]Department of Electrical Engineering and Computer Science, Massachusetts Institute of Technology, Cambridge, Massachusetts, USA. [7]Bruker Daltronics, Inc., Billerica, Massachusetts, USA. [8]New York University School of Medicine, New York University, New York, New York, USA. [9]Department of Biological Engineering, Massachusetts Institute of Technology, Cambridge, Massachusetts, USA. [10]Department of Chemistry and Integrative Genomics, Princeton University, Princeton, New Jersey, USA. [11]Department of Materials Science, Massachusetts Institute of Technology, Cambridge, Massachusetts, USA. [12]Department of Medical Oncology, Dana-Farber Cancer Institute and Harvard Medical School, Boston, Massachusetts, USA. [13]These authors contributed equally to this work. Correspondence should be addressed to M.G.V.H. (mvh@mit.edu).

Received 26 July; accepted 10 November; published online 26 December 2016; doi:10.1038/nm.4256

modified perfusion-based microfluidic strategy[22,23] in mice both with and without spontaneously arising pancreatic ductal adenocarcinoma (PDAC) (**Supplementary Fig. 1d**,**e**). PDAC was initiated by pancreas-restricted expression of Cre recombinase (*Pdx1-cre*) in *Kras*$^{LSL\text{-}G12D/+}$; *Trp53*$^{loxP/loxP}$ (KP) mice resulting in induction of mutant Kras G12D expression and loss of p53.

Following plasmapheresis of control (wild-type; WT) and KP mice, we achieved an initial enrichment in plasma of approximately 45% ± 9.2% labeled albumin (**Fig. 1a**), with minimal total protein loss from the plasma (**Supplementary Fig. 2a**). Despite slightly lower basal levels of protein in the plasma of KP mice as compared to WT mice, albumin levels were not different between the two groups, even when mice with a high tumor burden were in the end-stage phase of disease (**Supplementary Fig. 2b**). We reasoned that, if albumin is being catabolized, ^{15}N-labeled amino acids derived from albumin might be present in the plasma of these mice after plasma exchange (**Fig. 1b**). Increased levels of labeled alanine, leucine and phenylalanine were observed in the plasma of tumor-bearing KP mice as compared to WT control mice approximately 12 h after plasma exchange. This indicates the presence of albumin-derived amino acids in their blood and supports previous work suggesting that the rate of whole-body protein turnover is increased in KP mice with pancreatic tumors[24] (**Fig. 1b**). To determine the site(s) of albumin catabolism in tumors, we first examined labeled albumin peptides and free amino acids in normal pancreas from WT mice and in PDAC tissue from KP mice. Labeled albumin peptides were present at a higher concentration in tumor-derived tissue than in disease-free pancreas tissue, suggesting that uptake of labeled albumin increases in tumors (**Fig. 1c**). Next, we examined the amount of free amino acids in tumors and in normal pancreas following plasma exchange. We observed a significant increase in the amount of many labeled free amino acids in tumors when compared to normal pancreas, demonstrating that amino acids produced from the breakdown of labeled albumin are enriched in tumors when compared to disease-free pancreas (**Fig. 1d**).

To determine whether albumin-derived amino acids might be generated outside the pancreas through catabolism at distant sites, we examined labeled peptides and free amino acids in the liver, lung and muscle of normal (WT) and tumor-bearing (KP) mice (**Fig. 1e**,**f** and **Supplementary Fig. 2c–f**). In contrast to the findings in pancreatic tumors as compared to normal pancreas, we observed no significant increase in the levels of albumin peptides in the livers of mice with pancreatic cancer when compared to mice without pancreatic cancer (**Fig. 1e**). The abundance of some ^{15}N-labeled free amino acids was higher in the livers of mice with pancreatic cancer (**Fig. 1f**), and we observed elevated levels for some labeled free amino acids in the lungs of tumor-bearing mice (**Supplementary Fig. 2d**). However, increased levels of labeled amino acids were not detected in the skeletal muscle of mice with PDAC, and neither the lungs nor the skeletal muscle of mice with PDAC showed an increase in the abundance of albumin peptides (**Supplementary Fig. 2c**,**e**). Together, these findings suggest that pancreatic tumors uptake more albumin than normal pancreatic tissues and, further, that amino acids from the breakdown of albumin contribute more to the free amino acid supply in tumors than in normal pancreas. The presence of labeled amino acids in the liver and other organs (**Supplementary Fig. 2c–f**) leaves open the possibility that the labeling of amino acids in pancreatic tumor tissue results from local albumin catabolism and/or the uptake of free labeled amino acids derived from the breakdown of albumin in non-tumor tissues.

To determine whether tumor-autonomous catabolism of albumin is a feature of pancreatic tumors, we used an implantable device to deliver small and large molecules into solid tissues (**Fig. 2a**). The device was adapted from ref. 9 by modifying its diameter and reservoir sizes to allow for more effective release of large molecules into the pancreas. This device allows direct, controlled delivery of materials into the tumor microenvironment in a defined location that is trackable via microscopy. Macropinocytosis can be visualized by tracking the fate of fluorescently labeled high-molecular-weight (70-kDa) rhodamine-labeled dextran (Rh-dextran), a previously demonstrated marker of macropinocytosis[25]. Protein degradation is assessed by employing self-quenched BODIPY-labeled albumin (DQ-BSA), which becomes fluorescent upon enzymatic cleavage in the lysosomes of cells[26].

Devices loaded with 1 μg of Rh-dextran and DQ-BSA were implanted into subcutaneous xenografts derived from the MIA PaCa-2 (mutant RAS V12) and BxPC-3 (WT RAS) human PDAC cell lines. These two cells lines were previously reported to differ in their use of macropinocytosis for proliferation *in vivo*[7]. The implanted devices allowed local release of Rh-dextran and DQ-BSA adjacent to reservoirs 1 d after implantation (**Fig. 2b**). We tracked the fate of DQ-BSA and 70-kDa Rh-dextran delivered by the microdevices to investigate whether internalization of proteins by macropinocytosis in cells could be observed in these xenograft tumors (**Fig. 2b–d**). Twenty-four hours after device implantation, we observed high levels of dextran uptake and DQ-BSA fluorescence up to ~650 μm from the device in MIA PaCa-2 tumor tissue (**Fig. 2b**). The device also released dextran into BxPC-3 tumors, which exhibited a similar gradient of intratumoral release as MIA PaCa-2 tumors (**Fig. 2c**). Combined local release with 5-(*N*-ethyl-*N*-isopropyl)amiloride (EIPA), an agent known to inhibit the formation of macropinosomes[27], eliminated dextran uptake in MIA PaCa-2 tumors (**Fig. 2c**). We monitored DQ-BSA fluorescence over 2 d to determine whether the observed cellular uptake by tumor cells accompanied dextran diffusion and to examine further the kinetics of DQ-BSA degradation. Bright, narrow regions of fluorescence observed in MIA PaCa-2 tumors corresponding to local protein degradation appeared up to ~150 μm from the device by 24 h after device implantation (**Fig. 2d**). At 48 h after device implantation, fluorescent regions appeared at up to ~400 μm from the device (**Fig. 2d**). The observed diffusion distances are congruent with previously observed intratumoral release studies of several large and small molecules[9]. In contrast, intratumoral fluorescence from DQ-BSA was not observed when identical devices were placed into BxPC-3 xenograft tumors (**Fig. 2d**). These findings argue that local delivery of DQ-BSA allows examination of intratumoral albumin catabolism by macropinocytosis.

To determine whether we could observe uptake and catabolism of protein in real time, we used live multiphoton imaging of fluorescence from both DQ-BSA and 70-kDa Rh-dextran released from microdevices in MIA PaCa-2 and BxPC-3 tumors. We observed both uptake of dextran and an increase in the fluorescent signal from DQ-BSA in cells within MIA PaCa-2 xenograft tumors in mice (**Fig. 2e**). Dextran uptake was observed in the majority of tumor cells present within the exposed region at 1 h after implantation of the device. Uptake of albumin by tumor cells occurred at steady rates, with approximately two-thirds of the cells in an exposed region showing fluorescence corresponding to internalized Rh-dextran and DQ-BSA within 3 h of device implantation (**Fig. 2e**), a time consistent with the presence of albumin-derived amino acids observed in tumors in mice (**Fig. 1**). In contrast, the BxPC-3 cell line exhibited Rh-dextran labeling only of cell outlines, and few punctate spots from DQ-BSA were observed,

indicating minimal albumin degradation in these tumors (**Fig. 2e**). Images from the DQ-BSA studies were also used to determine the 'macropinocytic index', a metric previously described to quantify macropinocytosis in fixed samples[28]. By this metric, MIA PaCa-2 cells exhibited fourfold higher levels of macropinocytosis than BxPC3 cells (**Fig. 2f**).

To assess macropinocytosis and local protein degradation in KP tumors, we surgically implanted microdevices containing DQ-BSA directly into the pancreas of KP mice aged 8 weeks harboring autochthonous pancreatic tumors using a biopsy needle. In KP mice aged 8 weeks, the pancreas appears as a heterogeneous array of tumor and

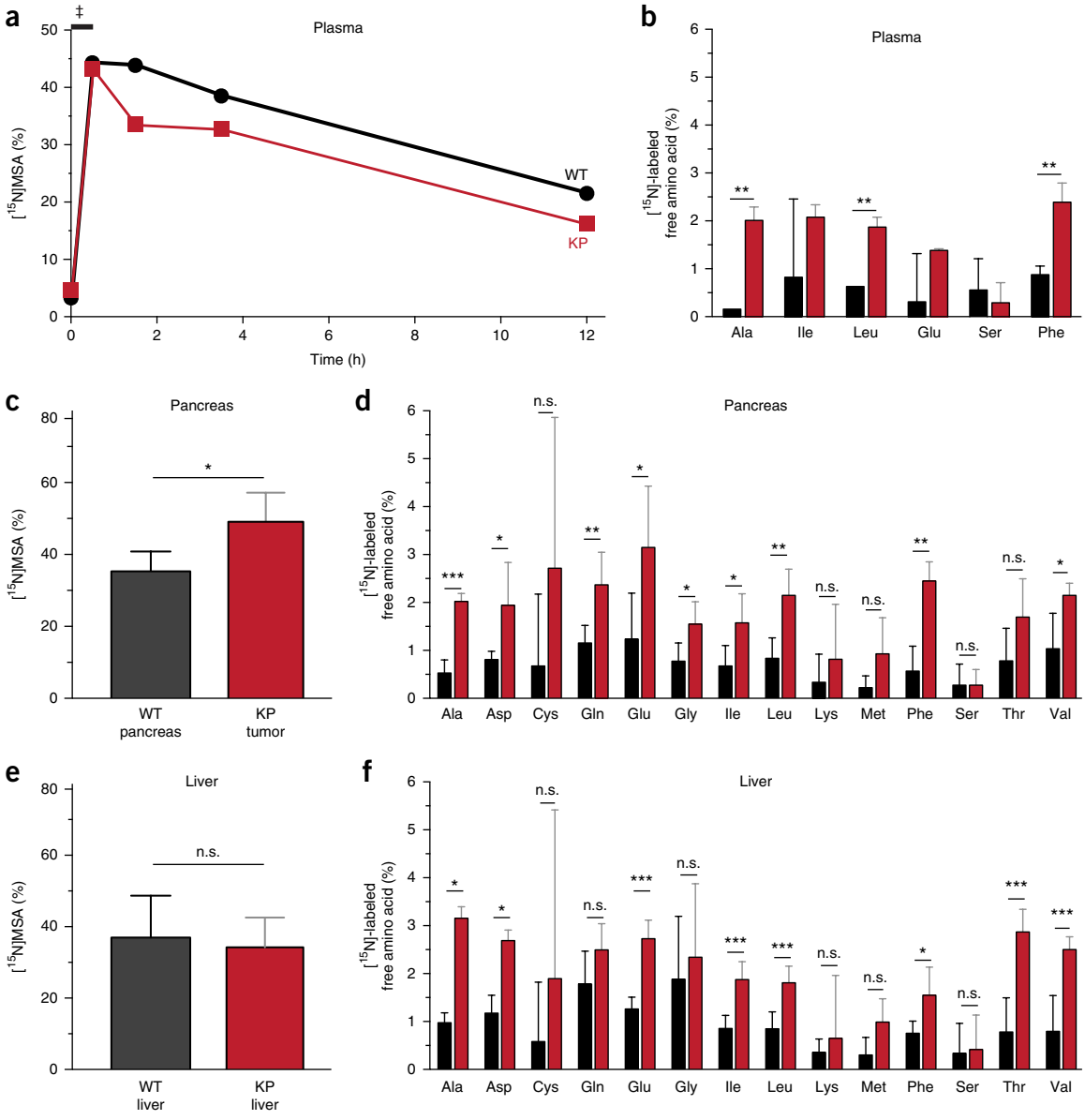

Figure 1 Albumin-derived amino acids are found in pancreatic tumors. (**a**) Representative albumin enrichment in the plasma of WT and KP mice following plasma exchange of [^{15}N]MSA for endogenous albumin. The percentage of [^{15}N]MSA determined by analysis of the albumin peptide LVQEVTDFAK in plasma by liquid chromatography coupled with tandem mass spectrometry (LC–MS/MS) over time is shown. The time point indicated by the double dagger corresponds to the 30-min period of plasma exchange. (**b**) Labeled amino acids in the plasma of WT and KP mice following plasma exchange of ^{15}N-labeled MSA for endogenous MSA. Plasma was sampled at the time of tissue collection (~12 h after exchange). The presence of ^{15}N-labeled amino acids was determined by gas chromatography coupled with mass spectrometry (GC–MS). (**c**) Following plasma exchange of ^{15}N-labeled MSA for endogenous MSA in WT and KP mice, the presence of [^{15}N]MSA in tissue was determined by analysis of multiple labeled peptides in normal pancreas (WT) and pancreatic tumors (KP) by LC–MS/MS. (**d**) Presence of labeled amino acids in pancreas tissue and tumors from WT and KP mice, respectively, following plasma exchange of ^{15}N-labeled MSA for endogenous MSA. Tissues were collected ~12 h after exchange, and the percentage of labeled amino acids was determined by GC–MS. (**e**) Following plasma exchange of ^{15}N-labeled MSA for endogenous MSA in WT and KP mice, the presence of [^{15}N]MSA in tissue was determined by analysis of multiple labeled peptides in the livers of mice with (KP) and without (WT) pancreatic tumors by LC–MS/MS. (**f**) Presence of labeled amino acids in the livers of WT and KP mice ~12 h after plasma exchange of ^{15}N-labeled MSA for endogenous MSA. The percentage of labeled amino acids was determined by GC–MS. $n = 5$ mice per genotype for all experiments. Data in **b**–**f** were analyzed by unpaired t test to identify significant differences: $^{*}P < 0.05$, $^{**}P < 0.01$, $^{***}P < 0.001$. n.s., not significant.

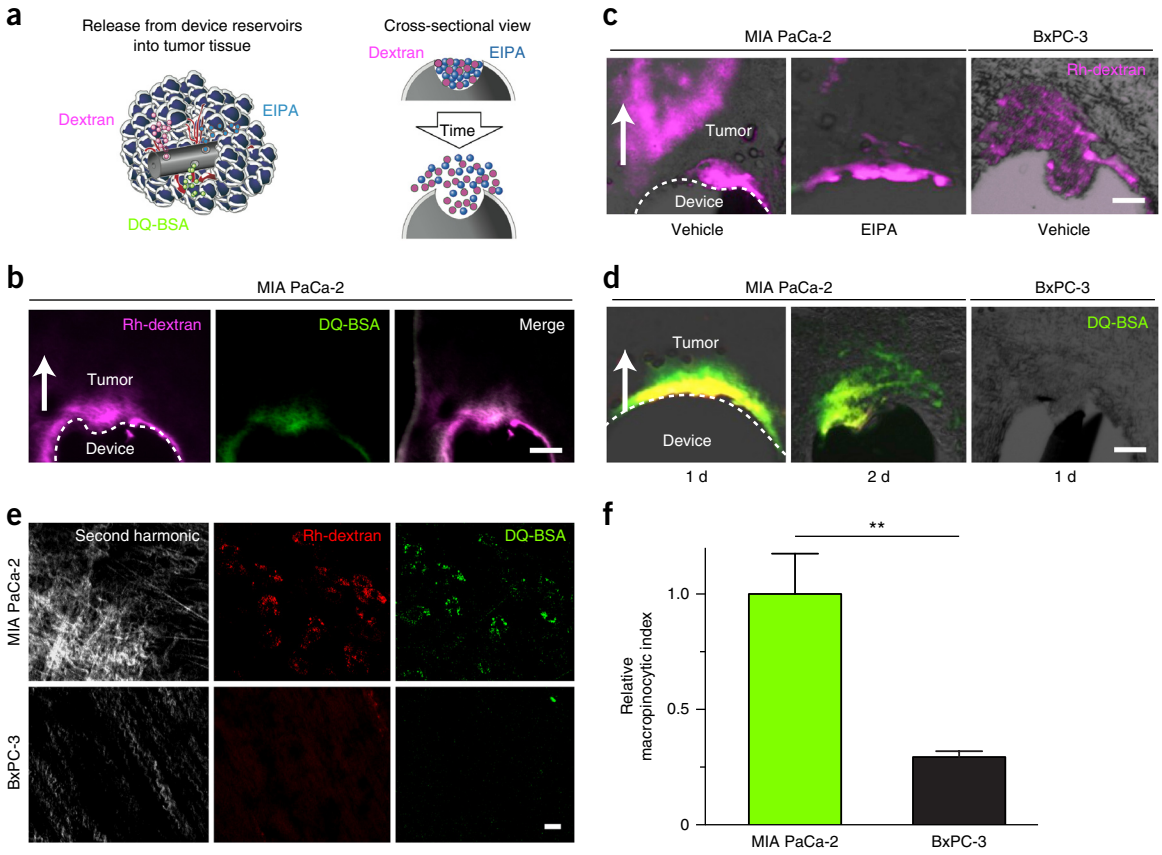

Figure 2 Direct assessment of macropinocytosis and albumin catabolism in tumors. (**a**) Schematic depicting devices implanted into tumors. Diffusion of specified contents radially outward from the reservoirs is shown in 3D (left) and cross-sectional (right) views. The orientation of the schematic on the right matches the orientation of device placement relative to tissue in **b**–**d**. (**b**) Microscopy to assess diffusion of 70-kDa Rh-dextran and DQ-BSA from a single device reservoir in MIA PaCa-2 tumors. Scale bar, 200 µm. (**c**) Microscopy to assess diffusion of 70-kDa Rh-dextran from an implanted device containing vehicle or EIPA, as indicated, into MIA PaCa-2 and BxPC-3 tumor tissue. Tissue was analyzed 48 h after device implantation. Scale bar, 150 µm. (**d**) Microscopy to assess fibrillar collagen (second harmonic) and fluorescence from DQ-BSA delivered from implanted devices to MIA PaCa-2 and BxPC-3 tumors. Scale bar, 200 µm. (**e**) Multiphoton microscopy to assess fluorescence from Rh-dextran and DQ-BSA delivered from implanted devices in MIA PaCa-2 and BxPC-3 tumors in live mice. The images were acquired 4 h after device implantation. Scale bar, 20 µm. (**f**) The macropinocytic index calculated based on DQ-BSA fluorescence in MIA PaCa-2 and BxPC-3 xenograft tumors. The macropinocytic index is the ratio of the total area of all macropinosomes in a field of designated area ($n = 5$ distinct fields per cell line). In **b**–**d**, white arrows indicate the direction of delivery of DQ-BSA, Rh-dextran or EIPA. Images are representative of six images from two mice per cell line per condition with triplicate reservoirs in **b**–**d** and two mice per cell line per condition with duplicate reservoirs in **e**. In **f**, data from two mice per cell line per condition with duplicate reservoirs were used to calculate macropinocytic index. Error bars, s.d. Data in **f** were analyzed by unpaired *t* test: $^{**}P < 0.01$.

normal tissue[24,29] (**Fig. 3a** and **Supplementary Fig. 3a**). Twenty-four hours after device delivery, tissue adjacent to device reservoirs containing DQ-BSA exhibited fluorescence only when the reservoirs were adjacent to tumor tissue (**Fig. 3a**). No fluorescence from DQ-BSA was detected in non-tumor pancreas regions, suggesting an absence of albumin degradation at these sites. We next sought to determine the kinetics of dextran uptake and DQ-BSA degradation, and whether these processes occur in cells with *Kras*^{G12D} activation within the pancreas. To distinguish Cre-expressing cells, we used multiphoton live microscopy in a KP mouse that also harbored a tdTomato$^{LSL/+}$ allele as a fluorescent marker of Cre recombinase activity and, therefore, *Kras*^{G12D} activation. Using multiphoton intravital microscopy, we observed a high degree of colocalization of the fluorescent tdTomato signal and the fluorescent DQ-BSA signal (**Fig. 3b**), and an increase in fluorescence due to DQ-BSA degradation was observed over a 90-min time period in tumor cells with tdTomato fluorescence (**Fig. 3c**,**d**). When a microdevice was introduced into a KP mouse lacking the tdTomato allele, comparable fluorescence from DQ-BSA was observed in tumor tissue, arguing that the observed DQ-BSA signal is not the result of overlap in the tdTomato and DQ-BSA emission/excitation spectra (**Supplementary Fig. 3b**). On the basis of DQ-BSA fluorescence, we further observed that spontaneous KP tumors exhibited a level of macropinocytosis comparable to that observed in MIA PaCa-2 xenografts (**Supplementary Fig. 3c**).

One hallmark of pancreatic tumors, including tumors found in KP mice, is a dense stroma that is rich in extracellular matrix (ECM)[30,31]. To determine whether tumor cells can internalize ECM-derived proteins, we used the microdevice to deliver TRITC-labeled fibronectin (440 kDa), which is one of the largest protein components of the ECM. Using intravital microscopy in live mice, we observed clear uptake of fibronectin in the tumor tissue of KP mice but not in WT pancreas (**Fig. 3e**). When considered together, these observations suggest that cells in spontaneously arising pancreatic tumors can consume protein in their environment.

Hydroxychloroquine is a lysosomal inhibitor being studied as a potential therapy for PDAC[32]. To determine whether we could

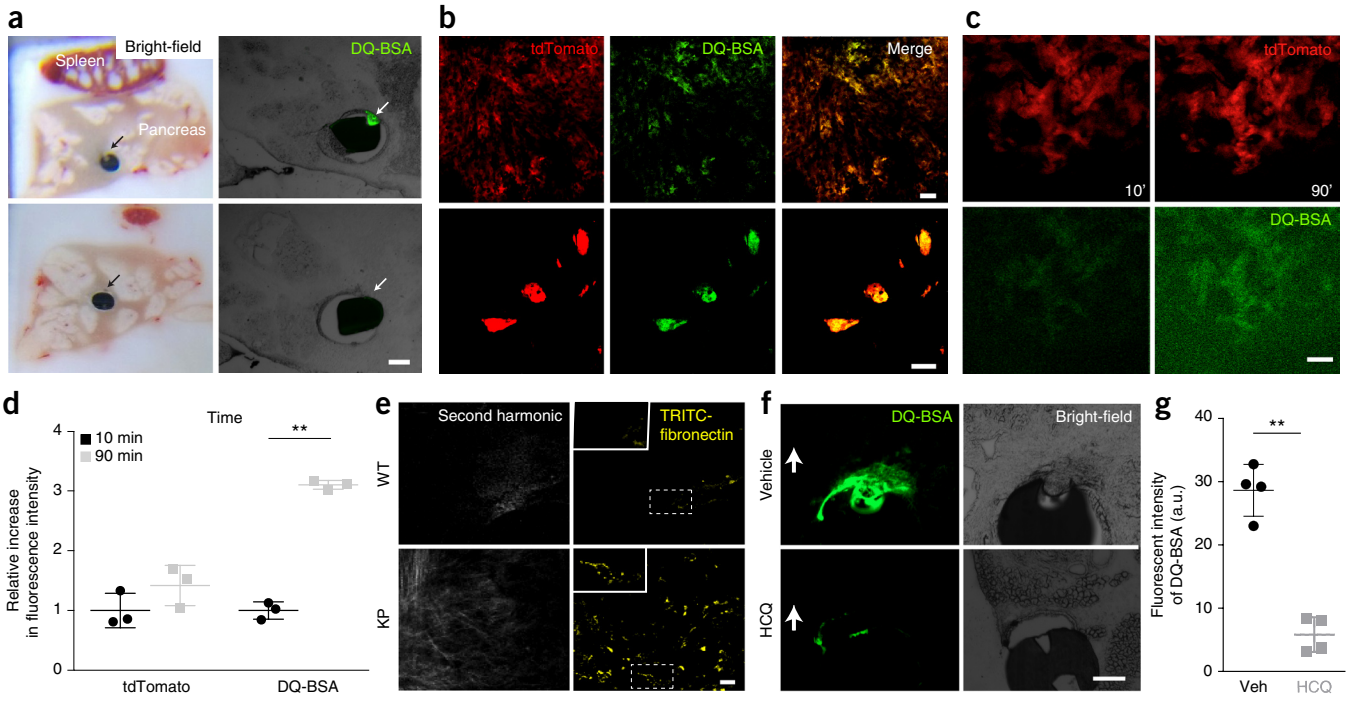

Figure 3 Albumin catabolism and fibronectin internalization in autochthonous pancreatic tumors. (**a**) Tissue sections with devices implanted to deliver DQ-BSA visualized by bright-field (left) and fluorescence (right) microscopy are shown. Arrows indicate reservoir position, and DQ-BSA fluorescence is shown in green. Scale bar, 1 mm. (**b**) Multiphoton microscopy to assess tdTomato and DQ-BSA fluorescence in pancreatic tumors in live KP mice harboring a tdTomato^{LSL} allele. DQ-BSA was delivered from an implanted device, and images were obtained 4 h after device implantation. Images acquired with low-power (top) and high-power (bottom) objectives are shown. Scale bars, 20 μm. (**c**) Multiphoton microscopy to assess the tdTomato and DQ-BSA fluorescence of pancreatic tumors in live KP mice harboring a tdTomato^{LSL} allele over time. Images obtained 10 and 90 min after device implantation are shown. Scale bar, 50 μm. (**d**) Quantification of DQ-BSA and tdTomato fluorescence in the experiment in **c** 10 and 90 min after implantation ($n = 2$ mice per genotype per condition with duplicate reservoirs). Error bars, s.d. (**e**) Multiphoton microscopy to assess fibrillar collagen (second harmonic) and TRITC-fibronectin fluorescence in normal pancreas (WT) and pancreatic tumor (KP) in live mice. Images were obtained 30 min after device implantation to deliver TRITC-fibronectin. Dashed boxes indicate the areas magnified in the insets to show the cellular distribution of TRITC-fibronectin. Scale bar, 20 μm. (**f**) Fluorescence and bright-field microscopy of pancreatic tumor tissue sections from KP mice in which devices were implanted to deliver DQ-BSA with vehicle or the lysosomal inhibitor hydroxychloroquine (HCQ). White arrows indicate the direction of release from reservoirs containing DQ-BSA and vehicle or hydroxychloroquine. Scale bar, 200 μm. (**g**) Quantification of the fluorescence intensity of DQ-BSA in the presence and absence of hydroxychloroquine. Veh, vehicle; a.u., arbitrary units. Error bars, s.d. Images are representative of two mice per cell line per condition with triplicate reservoirs in **a** and with duplicate reservoirs in **b**–**e**. Images are representative of five distinct tumor regions per condition in **f**. Data in **d** and **g** were analyzed by unpaired *t* test: $^{**}P < 0.01$.

inhibit catabolism of DQ-BSA, we delivered devices with reservoirs containing DQ-BSA and either vehicle or hydroxychloroquine. We observed decreased levels of DQ-BSA signal around reservoirs with hydroxychloroquine as compared to those with vehicle (**Fig. 3f**,**g**), suggesting that the lysosome is involved in the catabolism of DQ-BSA in PDAC cells in tumors.

To determine whether inhibiting macropinocytosis with EIPA has an effect on amino acid levels in pancreatic tumors, we implanted devices containing EIPA or a vehicle control into the pancreas of KP mice aged 7–8 weeks for 24 h. After tumor dissection, tissue slices adjacent to EIPA- or vehicle-containing reservoirs were analyzed using matrix-assisted laser desorption ionization coupled to imaging mass spectrometry (MALDI–IMS). This enabled the simultaneous measurement of EIPA distribution from the device into tumor tissue and spatial differences in the relative levels of amino acids within the tissue. We observed no change in the relative concentrations of choline, a metabolite that is not expected to be affected by EIPA treatment, in the tumor tissue regions that were exposed to EIPA (**Supplementary Fig. 4a**). A robust signal for the amino acids glutamate, aspartate, glutamine and histidine was also detected in the tissue slices. The relative concentrations of all four amino acids were lower in tissue exposed to EIPA than in adjacent tissue that was not exposed to EIPA, and amino acid levels were not different in tumor tissue exposed to vehicle alone (**Fig. 4** and **Supplementary Fig. 4b**). Notably, the regions of tissue analyzed were confirmed to be tumor tissue by H&E staining, with the relative concentrations of the amino acids detected found to be anticorrelated with regions of the tumor exposed to EIPA, suggesting that exposure to this compound resulted in local amino acid depletion (**Fig. 4a**,**b** and **Supplementary Fig. 4b**). In tumor regions adjacent to vehicle-containing, control reservoirs, the relative concentrations of aspartate and glutamate were uniform as compared to the rest of the tissue section (**Fig. 4c**). Using the orientation of device placement, we examined the approximate region of vehicle delivery to tumor tissue (400–500 μm), and no differences in aspartate or glutamate levels were observed around the predicted region of vehicle delivery (**Fig. 4d**). Thus, the decreased levels of amino acids in the EIPA-exposed regions of the tumor corroborate the hypothesis that tumors derive a meaningful fraction of their amino acids from catabolism of extracellular protein obtained by macropinocytosis.

EIPA inhibits macropinocytosis at the concentrations used for these studies[7,8]; however, EIPA is also an inhibitor of Na^+/H^+ exchange and

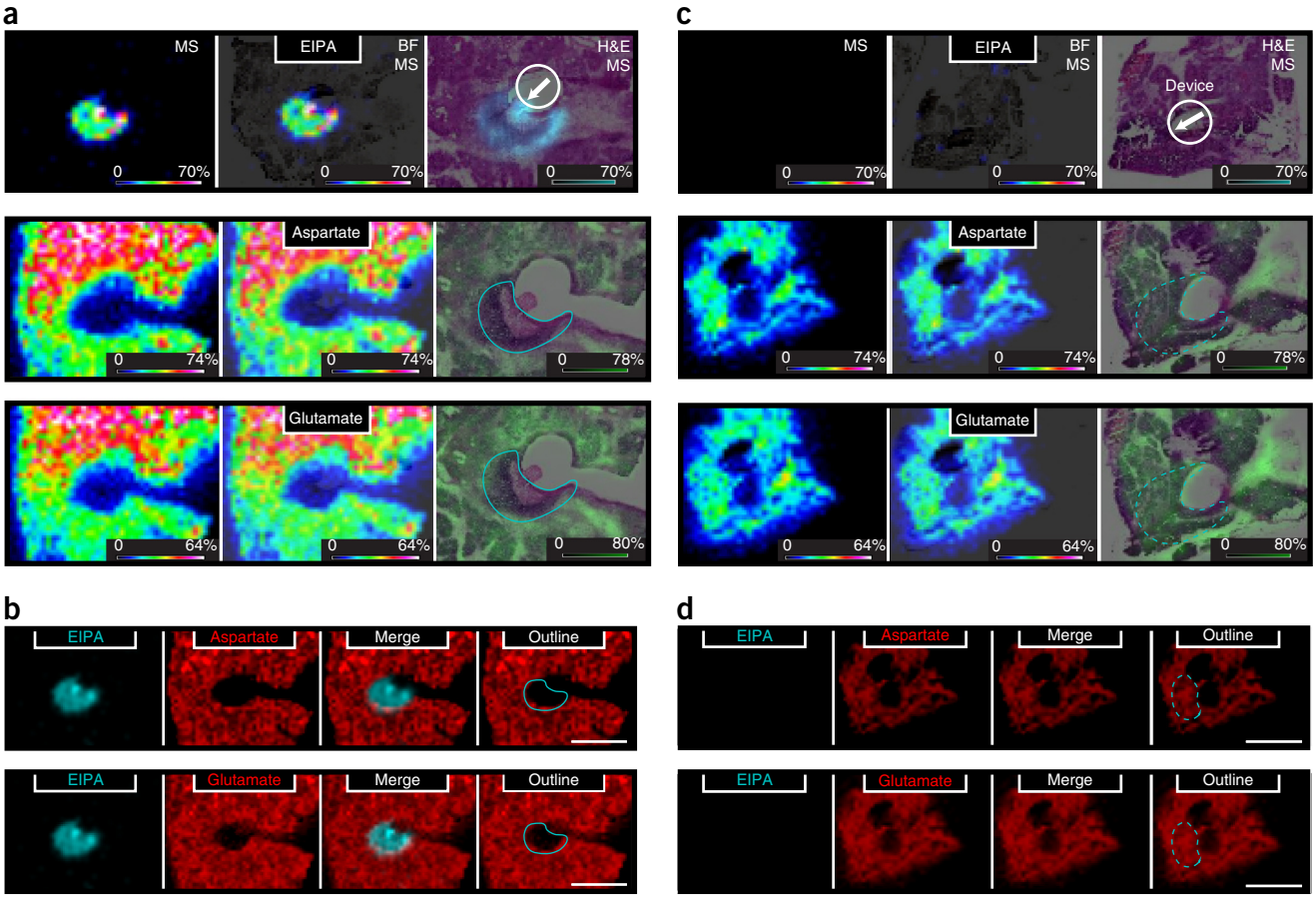

Figure 4 Local depletion of amino acids following inhibition of macropinocytosis in *Kras*^{G12D}-driven pancreatic tumors *in vivo*. (**a**) MALDI–IMS in positive ion mode was used to detect the macropinocytosis inhibitor EIPA (top; EIPA diffused approximately 400–500 μm from the device). Negative ion mode was used to detect the amino acids aspartate and glutamate (middle and bottom, respectively). Left images (MS) show only mass spectrometry signal, center images (BF, MS) show overlay of the mass spectrometry signal onto a bright-field image of an adjacent tissue section, and right images (H&E, MS) show overlay of the mass spectrometry signal onto H&E staining of an adjacent tissue section. A schematic showing device placement is included in the top right panel; the arrow indicates the direction of EIPA release. In the images to the right, the blue line outlines the region in which EIPA signal is detected. Scale bar, 1 mm. (**b**) Qualitative signal for EIPA (blue) and signal for the amino acids aspartate (top) and glutamate (bottom) (red) are shown in separate and overlaid images. An outline (blue line) of the area in which EIPA signal is detected is overlaid onto the images showing aspartate and glutamate signal. Scale bars, 1 mm. (**c**) Devices containing vehicle control (polyethylene glycol) were implanted directly into pancreatic tumors in KP mice. 24 h after device implantation, serial sections from the tumor were analyzed by MALDI–IMS. Positive ion mode was used to demonstrate absence of the macropinocytosis inhibitor EIPA (top; no EIPA observed, vehicle). Negative ion mode was used to detect the amino acids aspartate and glutamate (middle and bottom, respectively). Images are otherwise as described in **a**. Scale bar, 1 mm. (**d**) Qualitative signal for EIPA (blue) and signal from the amino acids aspartate (top) and glutamate (bottom) (red). Images are as described in **b**. Scale bars, 1 mm. Images are representative of two KP mice with triplicate reservoirs in **a** and **c**. The dashed blue line in **c** and **d** represents the predicted distance of vehicle diffusion.

may affect amino acid levels by other mechanisms. To test this possibility, we determined whether EIPA affected branched-chain amino acid (BCAA) levels under conditions where past work had shown that the acquisition of BCAAs was or was not dependent on macropinocytosis[6,33]. We found that BCAA levels were decreased when pancreatic cancer cells were cultured in medium lacking BCAAs, that BCAA levels could be rescued by providing cells with excess albumin and that the ability to rescue BCAA levels with albumin was inhibited by EIPA, although EIPA had no effect on BCAA levels otherwise (**Supplementary Fig. 4c**). We also assessed whether EIPA affected intracellular amino acid levels in pancreatic cancer cells in culture, where amino acids are freely available, and whether EIPA affected uptake of labeled amino acids from the medium. EIPA had no effect on the levels of most amino acids under these conditions (**Supplementary Fig. 4d,e**), including glutamine, glutamate and aspartate—three of the amino acids found to be depleted by EIPA in tumors. These data argue that, at the doses used, EIPA has minimal effect on the uptake or exchange of free amino acids and further strengthen our conclusion that macropinocytosis is important in the maintenance of amino acid levels within tumors.

In contrast to previous studies examining albumin synthesis and degradation by different organs in tumor-bearing animals[16,34], we provide direct evidence that pancreatic tumors catabolize albumin and derive a fraction of their amino acids from the breakdown of extracellular protein. Although these findings remain consistent with the breakdown of host tissue proteins contributing nutrients to pancreatic tumors[24], they further suggest that cancer cells in these tumors catabolize host-derived proteins in their environment. Hypoalbuminemia was not observed in KP mice, suggesting that the quantity of albumin catabolized by tumors is not sufficient to result directly in hypoalbuminemia over the timeframe during which the process was observed in this study within KP mice. However, the

increased turnover of whole-body protein stores and albumin consumption by tumors may eventually affect circulating albumin levels in patients with pancreatic cancer[13].

We report two methods to interrogate albumin catabolism that are possibly extendable to other solid tumors. Labeling of albumin on specific amino acids could also enable finer mapping of the fate of protein-derived amino acids in central carbon metabolism. Using albumin as a carrier for chemotherapeutics has been a successful therapeutic strategy in the clinic[10,35], possibly owing to the propensity of some tumors to use macropinocytosis. Albumin conjugation and preferential albumin uptake can allow for both better solubility and improved tumor delivery of therapeutic agents[36]. The approaches used here to study local protein catabolism may also allow for direct testing of therapeutic hypotheses in an individual tumor and could be used at the time of biopsy to identify patients who might benefit from treatments that take advantage of increased protein catabolism by tumors.

METHODS

Methods, including statements of data availability and any associated accession codes and references, are available in the online version of the paper.

Note: Any Supplementary Information and Source Data files are available in the online version of the paper.

ACKNOWLEDGMENTS

The authors wish to dedicate this paper to the memory of Katherine Kellersberger. We thank the MIT Department of Chemical Engineering and J. Francois-Hamel for access to bioreactor equipment, R. Bronson for pathological grading of tumors and A. Lau for providing tumor-bearing mice. S.M.D. and A.L. received support from a National Science Foundation Graduate Research Award Fellowship, and support from T32 GM007287 is also acknowledged. O.J. received support from the Koch Institute Frontier Grant and the Prostate Cancer Foundation. J.R.M. acknowledges support from grant F30CA183474 from the NCI and grant T32 GM007753 from NIGMS. M.A.K. and G.S. acknowledge support from NIH grants 1R01 DK075850-01 and 1R01 CA160458-01A1. M.G.V.H. acknowledges support from the Lustgarten Foundation, the Ludwig Center at MIT, the Broad Institute SPARC program, the Burroughs Wellcome Fund, SU2C and the NIH (P30 CA1405141, R01 CA168653). H.W.H. and J.H. acknowledge support by DARPA's Dialysis-Like Therapy (DLT) program under SSC Pacific grant N66001-11-1-4182. This work is also supported by the use of MIT's Microsystems Technology Laboratories.

AUTHOR CONTRIBUTIONS

Conceptualization: S.M.D., O.J. and M.G.V.H. Methodology: S.M.D., O.J., M.A.K., H.W.H., A.L., J.R.M., J.W., A.M.D., M.W., C.R.C., K.J.C., A.L., K.A.K., B.K.S., G.S., J.H. and D.B.-S. Formal analysis: S.M.D., O.J. and A.M.D. Investigation: S.M.D. and O.J. Writing original draft: S.M.D., O.J. and M.G.V.H. Visualization: S.M.D., O.J. and M.G.V.H. Supervision: M.J.C., R.L. and M.G.V.H. Funding acquisition: O.J., J.D.R., R.L. and M.G.V.H.

COMPETING FINANCIAL INTERESTS

The authors declare no competing financial interests.

1. Metallo, C.M. & Vander Heiden, M.G. Understanding metabolic regulation and its influence on cell physiology. *Mol. Cell* **49**, 388–398 (2013).
2. Mayers, J.R. & Vander Heiden, M.G. Famine versus feast: understanding the metabolism of tumors *in vivo*. *Trends Biochem. Sci.* **40**, 130–140 (2015).
3. White, E. Exploiting the bad eating habits of *Ras*-driven cancers. *Genes Dev.* **27**, 2065–2071 (2013).
4. Locasale, J.W. Serine, glycine and one-carbon units: cancer metabolism in full circle. *Nat. Rev. Cancer* **13**, 572–583 (2013).
5. Wise, D.R. & Thompson, C.B. Glutamine addiction: a new therapeutic target in cancer. *Trends Biochem. Sci.* **35**, 427–433 (2010).
6. Kamphorst, J.J. *et al.* Human pancreatic cancer tumors are nutrient poor and tumor cells actively scavenge extracellular protein. *Cancer Res.* **75**, 544–553 (2015).
7. Commisso, C. *et al.* Macropinocytosis of protein is an amino acid supply route in Ras-transformed cells. *Nature* **497**, 633–637 (2013).
8. Davidson, S.M. *et al.* Environment impacts the metabolic dependencies of Ras-driven non–small cell lung cancer. *Cell Metab.* **23**, 517–528 (2016).
9. Jonas, O. *et al.* An implantable microdevice to perform high-throughput *in vivo* drug sensitivity testing in tumors. *Sci. Transl. Med.* **7**, 284ra57 (2015).
10. Schilling, U. *et al.* Design of compounds having enhanced tumour uptake, using serum albumin as a carrier. Part II. *In vivo* studies. *Int. J. Rad. Appl. Instrum. B* **19**, 685–695 (1992).
11. Steinfeld, J.L. I^{131} albumin degradation in patients with neoplastic diseases. *Cancer* **13**, 974–984 (1960).
12. Rothschild, M.A., Oratz, M. & Schreiber, S.S. Regulation of albumin metabolism. *Annu. Rev. Med.* **26**, 91–104 (1975).
13. Gupta, D. & Lis, C.G. Pretreatment serum albumin as a predictor of cancer survival: a systematic review of the epidemiological literature. *Nutr. J.* **9**, 69 (2010).
14. Andersson, C., Iresjö, B.M. & Lundholm, K. Identification of tissue sites for increased albumin degradation in sarcoma-bearing mice. *J. Surg. Res.* **50**, 156–162 (1991).
15. Brenner, D.A., Buck, M., Feitelberg, S.P. & Chojkier, M. Tumor necrosis factor-α inhibits albumin gene expression in a murine model of cachexia. *J. Clin. Invest.* **85**, 248–255 (1990).
16. Fearon, K.C. *et al.* Albumin synthesis rates are not decreased in hypoalbuminemic cachectic cancer patients with an ongoing acute-phase protein response. *Ann. Surg.* **227**, 249–254 (1998).
17. Jewell, W.R., Krishnan, E.C. & Schloerb, P.R. Apparent cellular ingress of albumin in Walker 256 tumor and rat muscle. *Cancer Res.* **35**, 405–408 (1975).
18. Swanson, J.A. & Watts, C. Macropinocytosis. *Trends Cell Biol.* **5**, 424–428 (1995).
19. Daly, R. & Hearn, M.T.W. Expression of heterologous proteins in *Pichia pastoris*: a useful experimental tool in protein engineering and production. *J. Mol. Recognit.* **18**, 119–138 (2005).
20. Tolner, B., Smith, L., Begent, R.H.J. & Chester, K.A. Production of recombinant protein in *Pichia pastoris* by fermentation. *Nat. Protoc.* **1**, 1006–1021 (2006).
21. Merlot, A.M., Kalinowski, D.S. & Richardson, D.R. Unraveling the mysteries of serum albumin—more than just a serum protein. *Front. Physiol.* **5**, 299 (2014).
22. Hou, H.W. *et al.* Deformability based cell margination—a simple microfluidic design for malaria-infected erythrocyte separation. *Lab Chip* **10**, 2605–2613 (2010).
23. Hou, H.W. *et al.* A microfluidics approach towards high-throughput pathogen removal from blood using margination. *Biomicrofluidics* **6**, 024115 (2012).
24. Mayers, J.R. *et al.* Elevation of circulating branched-chain amino acids is an early event in human pancreatic adenocarcinoma development. *Nat. Med.* **20**, 1193–1198 (2014).
25. Racoosin, E.L. & Swanson, J.A. Macropinosome maturation and fusion with tubular lysosomes in macrophages. *J. Cell Biol.* **121**, 1011–1020 (1993).
26. Klionsky, D.J. Autophagy in mammalian systems, Part B. Preface. *Methods Enzymol.* **452**, xxi–xxii (2009).
27. Koivusalo, M. *et al.* Amiloride inhibits macropinocytosis by lowering submembranous pH and preventing Rac1 and Cdc42 signaling. *J. Cell Biol.* **188**, 547–563 (2010).
28. Commisso, C., Flinn, R.J. & Bar-Sagi, D. Determining the macropinocytic index of cells through a quantitative image-based assay. *Nat. Protoc.* **9**, 182–192 (2014).
29. Bardeesy, N. *et al.* Both $p16^{Ink4a}$ and the $p19^{Arf}$–p53 pathway constrain progression of pancreatic adenocarcinoma in the mouse. *Proc. Natl. Acad. Sci. USA* **103**, 5947–5952 (2006).
30. Whatcott, C.J. *et al.* Desmoplasia in primary tumors and metastatic lesions of pancreatic cancer. *Clin. Cancer Res.* **21**, 3561–3568 (2015).
31. Mahadevan, D. & Von Hoff, D.D. Tumor–stroma interactions in pancreatic ductal adenocarcinoma. *Mol. Cancer Ther.* **6**, 1186–1197 (2007).
32. Manic, G., Obrist, F., Kroemer, G., Vitale, I. & Galluzzi, L. Chloroquine and hydroxychloroquine for cancer therapy. *Molecular & Cell. Oncol.* **1**, e29911–e29912 (2014).
33. Palm, W. *et al.* The utilization of extracellular proteins as nutrients is suppressed by mTORC1. *Cell* **162**, 259–270 (2015).
34. Andersson, C., Lönnroth, C., Moldawer, L.L., Ternell, M. & Lundholm, K. Increased degradation of albumin in cancer is not due to conformational or chemical modifications in the albumin molecule. *J. Surg. Res.* **49**, 23–29 (1990).
35. Von Hoff, D.D. *et al.* Increased survival in pancreatic cancer with nab–paclitaxel plus gemcitabine. *N. Engl. J. Med.* **369**, 1691–1703 (2013).
36. Wosikowski, K. *et al. In vitro* and *in vivo* antitumor activity of methotrexate conjugated to human serum albumin in human cancer cells. *Clin. Cancer Res.* **9**, 1917–1926 (2003).

ONLINE METHODS

Animal statement. All mouse studies were approved by the MIT Committee on Animal Care. Mice were housed under standard 12-h light/12-h dark cycles and fed RMH 3000 (Prolab) *ad libitum* until experiments were conducted. All experimental groups were assigned on the basis of genotype, and experiments were conducted with blinding. Plasma exchange experiments were all conducted at the same time of day. Cohort sizes were based on anticipated results from previous studies *in vitro*[8]. Mice were included in cohorts based on genotype.

Production of [^{15}N]MSA. *Alb* (mouse serum albumin; NM_009654.4) cDNA was cloned from the liver of a wild-type mouse using the following PCR primers: F, 5′-GAAGCACACAAGAGTGAGATCGC-3′; R, 5′-TTAGGCTAAGGC GTCTTTGCATCTA-3′. The cDNA was cloned into an expression vector containing α-factor and a *Gpd* (GAPDH) promoter from *P. pastoris* (pGAPZα) for subsequent transformation and expression in *P. pastoris* (Invitrogen). *P. pastoris* expressing MSA were cultured in a glucose fed-batch bioreactor (Sartorius) at 30 °C for 7 d with ^{15}N-labeled nutrients using conditions described previously[37]. Medium containing MSA was separated from the cellular fraction after centrifugation at 15,000*g* for 3 h at 4 °C, and supernatant containing MSA was concentrated using a rotary evaporator. Concentrated supernatant was dialyzed using a dialysis cassette with a 45-kDa molecular weight cutoff (Thermo Fisher) and further purified using a Q-Sepharose High-Performance anion-exchange column (GE). Purified MSA was subsequently lyophilized, resuspended in PBS and filtered through 0.45-µm filters for use in mouse experiments. Additional [^{15}N]MSA was acquired from Albumin Biosciences.

Microfluidic plasmapheresis device. The plasma-exchange microfluidic device is based on the concept of cell margination and was previously developed for bacterial clearance in a mouse model of sepsis[22,23]. The device is made of polydimethylsiloxane (PDMS) (Sylgard 184, Dow Corning) and consists of three channels: each channel is 6 mm long, 20 µm × 40 µm (width × height), with three stages of bifurcation at intervals of 2 mm along the channel length. A filter region with an array of square pillars (with 100-µm spacing) is added upstream of the margination channels to trap large thrombi or cell clusters to ensure smooth flow within the device. As blood flows through the margination channel, deformable red blood cells (RBCs) migrate axially toward the channel center, leaving a layer of plasma next to the channel wall, which is removed via the smaller side channels. To minimize RBC loss, the volume subjected to side-channel skimming is progressively lower (15%, 10%, 5%) at each bifurcation stage, with a total volume of ~30%. Therefore, the microdevice is capable of exchanging up to ~30% of plasma from incoming blood with labeled albumin, which is infused into the filtered blood through a separate syringe pump. During extracorporeal plasma exchange in mice, blood is drawn from an arterial (carotid) catheter, using a peristaltic pump (P720, Instech Laboratories) for ~25 min (30 µl min^{-1}), into the device, partially replacing the filtered blood with labeled albumin (10 µl min^{-1}) prior to its return to the mouse through a venous (jugular) catheter.

Mouse pancreatic cancer models. In the autochthonous genetically engineered mouse model of PDAC, tumors were initiated using a pancreas-restricted *Pdx1* promoter to express Cre recombinase (*Pdx1-cre*) in *Kras*$^{LSL\text{-}G12D/+}$; *Trp53*$^{loxP/loxP}$ mice from a mixed 129/Sv and C57BL6/J background. For imaging studies, tdTomato$^{LSL/+}$ mice were used to allow visualization of individual cells where Cre was expressed. Chronic catheters were implanted in the jugular vein and carotid artery when male mice were between 6–8 weeks of age with detectable tumors. For xenograft studies, male C57BL6/J or *nu*/*nu* mice aged 2–4 months were used. Briefly, 2.5 × 10^5 cells from established cell lines derived from C57BL6/J KP mice or 5 × 10^5 cells from the MIA PaCa-2 and BxPC-3 human pancreatic cancer cell lines were injected into the flanks of recipient mice, and experiments were performed when the total tumor volume was approximately 1 cm^3. All human cell lines were acquired from ATCC and cultured in 21% oxygen in DMEM containing 10% FBS and penicillin-streptomycin.

Metabolite extraction. Tissues were weighed (wet tissue weight) and homogenized cryogenically (Retsch Cryomill). Metabolites were extracted from tissues weighing between 10–40 mg in a chloroform:methanol:water extraction solution with a volume ratio of 400:600:300. Samples were vortexed and centrifuged at 10,000*g* for 10 min to separate the aqueous and organic layers. Polar metabolites were dried under nitrogen gas and frozen at −80 °C for subsequent analysis by gas chromatography coupled with mass spectrometry (GC–MS).

Measurement of labeled albumin peptides. Mouse tissue was extracted and homogenized in ice-cold 8 M urea. Proteins were quantified by BCA assay (Pierce). Proteins were reduced (10 mM dithiothreitol, 56 °C for 45 min) and alkylated (50 mM iodoacetamide, room temperature in the dark for 1 h) and were subsequently digested with trypsin (sequencing grade, Promega) at an enzyme:substrate ratio of 1:50 at room temperature overnight in 100 mM ammonium acetate, pH 8.9. Trypsin activity was quenched by the addition of formic acid to a final concentration of 5%. Peptides were desalted using C18 SpinTips (Protea) and were then lyophilized and stored at −80 °C. After being resuspended in 0.1% formic acid, each sample (1 µg of tissue or 100 ng of serum) was separated by reverse-phase HPLC using an EASY- nLC1000 (Thermo) over a 75-min gradient before nanoelectrospray using a QExactive mass spectrometer (Thermo). The mass spectrometer was operated in a data-dependent mode. The parameters for the full MS scan were as follows: resolution of 70,000 across *m*/*z* ratios of 350–2,000, AGC of 3 × 10^6 and maximum IT of 50 ms. The full MS scan was followed by MS/MS for the top ten precursor ions in each cycle with an NCE of 28 and dynamic exclusion of 30 s. Raw MS data files (.raw) were searched using Proteome Discoverer (Thermo) and Mascot version 2.4.1 (Matrix Science). The Mascot search parameters were as follows: mass tolerance of 10 ppm for precursor ions, fragment ion mass tolerance of 0.8 Da, two missed cleavages of trypsin, carbamidomethylation as the fixed modification and oxidized methionine as the variable modification. We analyzed the following peptides and all possible isotopomers to determine the plasma enrichment and quantity of labeled albumin in each tissue: AADKDTcFSTEGPNLVTR (+2), AADKDTcFSTEGPNLVTR (+3), APQVSTPTLVEAAR (+2), ENYGELADccTK (+2), LVQEVTDFAK (+2), SLHTLFGDK (+2) and TcVADESAANcDK (+2) (where c represents carbamidomethylation). Fractional enrichment was determined for each peptide, and each measurement represents the mean for the seven peptides. The average fractional enrichment in plasma and tissues was normalized to the average fractional plasma enrichment of [^{15}N]MSA after plasma exchange.

Gas chromatography and mass spectrometry measurement of free amino acids. 10 mg of dried tissue metabolites was dissolved in 10 µl of 2% methoxyamine hydrochloride in pyridine (Sigma) and held at 37 °C for 1.5 h. *tert*-butyldimethylsilyl derivatization was initiated by the addition of 15 µl of *N*-methyl-*N*-(*tert*-butyldimethylsilyl)trifluoroacetamide + 1% *tert*-butyldimethylchlorosilane (Sigma), and samples were incubated at 37 °C for 1 h. GC–MS analysis was performed using an Agilent 7890 gas chromatographer equipped with 30 m of DB-35MS capillary column connected to an Agilent 5975B mass spectrometer operating under electron impact ionization at 70 eV. One microliter of sample was injected in splitless mode at 270 °C, using helium as a carrier gas at a flow rate of 1 ml min^{-1}. For measurement of polar metabolites, the oven temperature was held at 100 °C for 3 min and increased to 300 °C at a rate of 3.5 °C min^{-1}. The mass spectrometer source and quadrupole were held at 230 °C and 150 °C, respectively, and the detector was run in scanning mode, recording ion abundance in the range of 100–605 *m*/*z*. Mass-isotopomer distributions (MIDs) were determined by integrating the appropriate ion fragments and were corrected for natural isotope abundance using in-house algorithms adapted as previously reported (METRAN, Matlab 2013b)[7]. Labeled amino acids were defined as *M* + 1 (one nitrogen labeled) and *M* + 2 (two nitrogens labeled) isotopomers of the examined amino acids for ^{15}N labeling studies or as *M* + *n* isotopomers (where *n* is the total number of carbon atoms composing each amino acid) for ^{13}C labeling studies.

Albumin measurements in plasma. Plasma was collected in EDTA-coated tubes, aliquotted and frozen at −80 °C for further analysis. Plasma mouse albumin levels were determined using a mouse albumin ELISA according to the manufacturer's specifications (Abcam, ab108791).

doi:10.1038/nm.4256

Device to deliver FITC DQ-BSA, Rh-dextran, FITC-dextran, TRITC-fibronectin, EIPA and hydroxychloroquine. Microdose drug delivery devices were manufactured as described previously[9]. In short, cylindrical microscale devices with dimensions 820 μm (diameter) × 4 mm (length) were manufactured from medical-grade Delrin acetyl resin blocks (DuPont) by micromachining (CNC Micromachining Center). Circular reservoirs (2–6 per device) were shaped on the outer surface of devices with dimensions 300 μm (diameter) × 250 μm (depth). DQ-BSA, dextran, fibronectin and/or hydroxychloroquine or EIPA (1 μg per reservoir) was packed into device reservoirs using a tapered metal needle (Electron Microscopy Sciences). Devices were implanted directly into mouse tumors with a 19-gauge spinal biopsy needle (Angiotech), using the retractable needle obturator to push the device into tissue. Devices remained *in situ* for 6–48 h. The tumor was then excised, and the tissue containing the device was snap frozen. Tissue was sectioned using a standard cryotome, and tissue slices of 20 μm in thickness were collected from each reservoir and imaged on an EVOS microscope.

Multiphoton imaging of DQ-BSA, FITC-dextran, Rh-dextran and TRITC-fibronectin. Intravital multiphoton imaging was performed as described previously[38] using a ×25 1.05 NA water immersion objective with a correction lens. 90-min time-lapse movies were analyzed to measure and quantify fluorescence intensity and cell characteristics in 3D and through time using NIH ImageJ[39]. Data were pooled from at least 3 mice per tumor group, with 4–8 fields imaged per mouse. The macropinocytic index was determined as previously described for xenograft tumors[28].

MALDI imaging experiments. Samples were cryosectioned at 20 μm and thaw mounted on glass slides; serial sections were analyzed. The orientation of the specimens was shifted for serial sections analyzed in positive versus negative ion mode, with device location used to orient the sample in each serial section. Slides were then coated with HCCA (7 mg ml^{-1}; 50% methanol, 0.1% TFA) or 9-aminoacridine (10 mg ml^{-1}; 70% ethanol, 0.1% TFA) using a TM sprayer (HTX Technologies). Serial sections were prepared for imaging analysis in both positive and negative ion modes on a 7T solariX-XR FTMS (Bruker) equipped with a dual ESI/MALDI source, a SmartBeam II 2-kHz Nd:YAG (355-nm) laser and paracell. Samples were analyzed with a raster width of 125 μm in positive ion mode and 100 μm in negative ion mode in the mass range of 80–2,000 m/z at an acquisition size of 2MW. Images contained 7,200–10,500 pixels. Data were visualized, and co-registration of H&E images was performed using FlexImaging 4.1. Compound identifications were made on the basis of accurate mass (<1 ppm difference from expected mass) and isotopic peak matching.

Cell culture. Cell lines from murine KP pancreatic tumors were established by standard protocols[24]. Cells were cultured in complete DMEM with 10% FBS and 5% penicillin-streptomycin. For BCAA deprivation, DMEM with 5% dialyzed serum with or without BCAAs (leucine, valine and isoleucine) was used in the presence or absence of 3% albumin and in the presence or absence of 20 μM EIPA. Where indicated, 2 mg ml^{-1} of a fully labeled ^{15}N- or ^{13}C-labeled amino acid mixture (Cambridge Isotopes Laboratories) was included for 6 h before metabolite extraction. Cells were tested and confirmed negative for mycoplasma before use.

Statistical analysis. Two-tailed unpaired Student's *t* tests were performed for all experiments, and data were normally distributed for all analyses conducted. Variances were not statistically different in any of the data. Results for independent experiments are presented as means ± s.d. unless otherwise stated.

37. Cregg, J.M., Cereghino, J.L., Shi, J. & Higgins, D.R. Recombinant protein expression in *Pichia pastoris*. *Mol. Biotechnol.* **16**, 23–52 (2000).
38. Wyckoff, J., Gligorijevic, B., Entenberg, D., Segall, J. & Condeelis, J. High-resolution multiphoton imaging of tumors *in vivo*. *Cold Spring Harb. Protoc.* **2011**, 1167–1184 (2011).
39. Sahai, E. *et al.* Simultaneous imaging of GFP, CFP and collagen in tumors *in vivo* using multiphoton microscopy. *BMC Biotechnol.* **5**, 14 (2005).